NASA Technical Memorandum 87063

Reverberation Effects on Directionality and Response of Stationary Monopole and Dipole Sources in a Wind Tunnel

Kenneth J. Baumeister
Lewis Research Center
Cleveland, Ohio

Prepared for the
1985 Winter Annual Meeting of the
American Society of Mechanical Engineers
Miami Beach, Florida, November 17–21, 1985

NASA

REVERBERATION EFFECTS ON DIRECTIONALITY AND RESPONSE OF STATIONARY MONOPOLE AND DIPOLE SOURCES IN A WIND TUNNEL

Kenneth J. Baumeister
National Aeronautics and Space Administration
Lewis Research Center
Cleveland, Ohio 44135

ABSTRACT

Analytical solutions for the three-dimensional inhomogeneous wave equation with flow in a hardwall rectangular wind tunnel and in the free field are presented for a stationary monopole noise source. Dipole noise sources are calculated by combining two monopoles 180° out of phase. Numerical calculations for the modal content, spectral response and directivity for both monopole and dipole sources are presented. In addition, the effect of tunnel alterations, such as the addition of a mounting plate, on the tunnels reverberant response are considered. In the frequency range of practical importance for the turboprop response, important features of the free field directivity can be approximated in a hardwall wind tunnel with flow if the major lobe of the noise source is not directed upstream. However, for an omnidirectional source, such as a monopole, the hardwall wind tunnel and free field response will not comparable.

E-2432

INTRODUCTION

The relatively high fuel economy available from propeller-driven aircraft has renewed interest in high speed, highly loaded multiple blade turboprop propulsion systems. The undesirable features of community noise and, more importantly, the high intensity cabin noise associated with the propellers supersonic helical tip speeds have stimulated new theoretical and experimental research on the acoustic characteristics of turboprops.

The acoustic testing of propellers at realistic inflow Mach numbers can be carried out in flight using a suitably scaled model, or performed in a wind

tunnel capable of producing high subsonic flow velocities, again using a scale model. Since the cost of flight testing is high, acoustic testing with supersonic helical tip speed propellers has initially been carried out in the 8 by 6 ft transonic wind tunnel at the Lewis Research Center (1-6). Figure 1 displays typical propeller models mounted in the Lewis 8 by 6 wind tunnel. The propeller is driven at the desired speed by an air drive. Noise measurements are made with pressure transducers installed flush with the tunnel walls, through the bleed holes shown in the photograph or on added structures such as the boundary layer refraction plate. As seen in Fig. 1, the hard tunnel wall, wings, or refraction plates could produce significant reverberation effects; thus, the accuracy of the noise measurements has been questioned. In measurements of this type, the test site is essentially a duct containing a noise source represented by the propeller. It is not clear that this test environment will generally produce results for directivity or amplitude which have any relationship to flight test results, although some initial flight to wind tunnel comparisons with the NASA Dryden Jet star aircraft (7,8) have indicated reasonable agreement.

Dittmar (9) has qualitatively argued that flow convection and the highly directional nature of a typical propeller noise source will minimize reverberation effects when the tunnel Mach number is greater than 0.6. However, Eversman and Baumeister (10) found the acoustic radiation field to be substantially altered by the presence of the duct except perhaps very near the propeller. They found a strong resemblance between the acoustic directivity on the duct wall and the general shape of the free field directivity for side line angles of 45° to 135°. For side line angles less than 45° or greater than 135°, similarity between duct directivity and free field could not be expected.

Because of computer storage limitations, the results of Ref. 10 were based on axial Mach numbers less than -0.5 and source frequencies approximately 25 percent of the turboprop test frequency (1000 Hz). Considerations in this paper will be given to the actual rectangular form of the 8 by 6 Lewis wind tunnel, the design frequency (1000 Hz) and the design Mach number of 0.8.

It is the purpose of the present investigation to mathematically model in closed form the radiation patterns of stationary monopoles and dipoles in a hard wall version of the NASA 8 by 6 wind tunnel, in free space, and in a half space adjacent to a solid infinite plane. In contrast to the cylindrical geometry and low frequency results of Ref. 10, the acoustic response for the NASA 8 by 6 wind tunnel will be determined for a rectangular geometry in the frequency range associated with the first harmonic of the propeller tests (1000 Hz).

The analysis to follow models the pressure solutions for a stationary monopole in an infinite duct with flow. First, the appropriate governing wave equations and boundary conditions will be presented and solved. Next, the free field pressure solutions for a monopole source as given by Goldstein (11) is developed in terms of the duct coordinate system. These solutions are used to describe the resonance frequencies and modal amplitudes of the 8 by 6 wind tunnel. Finally, for a monopole and dipole source in the tunnel, the spectral response, directionality, and spectral response changes due to the addition of panels or other superstructure into the tunnel are determined.

NOMENCLATURE

A	constant of integration
a	integer index, see Eq. (A51)
B	constant of integration
b	integer index, see Eq. (A51)
C	constant of integration

c	dimensionless sonic velocity, c^*/H^*f^* Eq. (4)
D_o	dipole strength
f^*	frequency, Hz
H^*	tunnel height, m
i	$\sqrt{-1}$
K_{nm}	defined Eq. (8)
k	wave number, ω/c
k_x, k_y, k_z	wave number in respective coordinates
L	dimensionless tunnel width, L^*/H^*
M	Mach number, U^*/c^*
M_o	Mach number V/c
M_s	source Mach number
m	transverse "z" mode number
N_m	number of m modes
N_n	number of n modes
n	transverse mode number
P	dimensionless acoustic pressure, P^*/ρ^*c^{*2}
Q_o	time independent monopole source strength
q	dimensionless monopole strength, $(H^*/c^*)q^*$
q_o	spatially independent monopole source strength
Re	equivalent radius, defined Eq. (21)
r	radius
r_s	source radius, defined Eq. (24)
T^*	period, sec
t	dimensionless time. t^*/T^*
U	axial mean velocity, $cM = U^*/H^*f^*$
V	negative image of axial velocity, $- U$
v	dimensionless acoustic velocity, see Eq. (2)

X	function of x
x	dimensionless axial coordinate, x^*/H^*
Y	function of y
y	dimensionless transverse coordinate, y^*/H^*
Z	function of z
z	dimensionless transverse coordinate, z/H^*
α_{nm}	mode factor, Eqs. (11) and (12)
β_m	defined Eq. (17)
β_n	defined Eq. (16)
γ	Mach number convection factor, Eq. (13)
δ	delta function
θ	source-observer angle, defined Eq. (20)
φ	dimensionless perturbation velocity potential, ϕ^*/c^*H^*
Ψ	eigen-function
ω	dimensionless angular velocity, $2\pi f^*T^*$

Subscripts

f	fixed coordinates
g	Galilean coordinates
m	transverse "z" mode number
n	transverse "y" mode number
o	space independent
s	source position
+	positive x direction
-	negative x direction

Superscripts

*	dimensional quantity
'	coordinate system Eq. (A11)
"	coordinate system, Eq. (A25)

WIND TUNNEL MATHEMATICAL MODEL

The first solution to be presented is for a stationary monopole source in a duct with flow as shown in Fig. 2. The equations and boundary conditions describing the sound propagation will now be presented along with their solutions.

Governing Equations

The linearized gas-dynamic equations for a monopole noise source are given by Goldstein ((11), Eq. (1.11)) in vector form. For the rectangular duct in the fixed coordinate system of Fig. 2, these equations can be combined to obtain a dimensionless wave equation of the following form:

$$(1 - M^2)\frac{\partial^2\varphi}{\partial x_f^2} + \frac{\partial^2\varphi}{\partial y_f^2} + \frac{\partial^2\varphi}{\partial z_f^2} - \frac{2M}{c}\frac{\partial^2\varphi}{\partial t_f \partial x_f} - \frac{1}{c^2}\frac{\partial^2\varphi}{\partial t_f^2} = q \tag{1}$$

where

$$v_x = \frac{\partial\varphi}{\partial x_f} \qquad v_y = \frac{\partial\varphi}{\partial y_f} \qquad v_z = \frac{\partial\varphi}{\partial z_f} \tag{2}$$

and

$$p = -\frac{1}{c}\frac{\partial\varphi}{\partial t_f} - M\frac{\partial\varphi}{\partial x_f} \tag{3}$$

The usual notation for velocity potential, acoustic velocity, and acoustic pressure are used. These and other symbols are defined in the nomenclature. Here, the dimensionless speed of sound c is defined as

$$c = \frac{c^*}{H^* f^*} \tag{4}$$

The asterisks denote dimensional quantities.

For a monopole source, wave Eq. (1) can be rewritten as

$$(1 - M^2)\frac{\partial^2\varphi}{\partial x_f^2} + \frac{\partial^2\varphi}{\partial y_f^2} + \frac{\partial^2\varphi}{\partial z_f^2} - \frac{2M}{c}\frac{\partial^2\varphi}{\partial x_f \partial t_f} - \frac{1}{c^2}\frac{\partial^2\varphi}{\partial t_f^2}$$

$$= q_0(t_f)\delta(x_f)\delta(y_f - y_s)\delta(z_f - z_s) \tag{5}$$

The solution to Eq. (5) can be more conveniently obtained by first rewriting Eq. (5) in a Galilean (x_g, y_g, z_g, t_g) system moving with the flow, and then transforming into a Lorentz coordinate system, as outlined by Morse and Ingard ((12), pp. 701 and 722). The standard separation of variable solution in the Lorentz system and transform back into the tunnel coordinate system shown in Fig. 2 yields

$$P(x,y,z,t) = \frac{Q_o}{2L} \left\{ \sum_{n=0}^{N_y+5} \sum_{m=0}^{N_z+5} \frac{\Psi_{nm}(y,z)\Psi_{nm}(y_s,z_s)}{\beta_n \beta_m \alpha_{nm} K_{nm}} \gamma^2 \left[1 - M\alpha_{nm}K_{nm}\,\mathrm{sgn}(x - x_s)\right] \right.$$
$$\left. \times \exp\left[\frac{i\omega}{c}(x - x_s)\gamma^2(\alpha_{nm}K_{nm}\,\mathrm{sgn}(x - x_s) - M\right]\right\} e^{-i\omega t} \qquad (6)$$

where

$$\omega^* = 2\pi f^* \quad \text{or} \quad \omega = 2\pi \qquad (7)$$

(the frequency f^* is tied to the definition of $t = f^*t^*$ in the dimensionless representation of ω)

$$K_{nm} = \sqrt{\left|1 - \left(\frac{n\pi c}{\gamma\omega}\right)^2 - \left(\frac{m\pi c}{\gamma L\omega}\right)^2\right|} \qquad (8)$$

$$\Psi_{nm}(y,z) = \cos(n\pi y)\cos\left(\frac{m\pi z}{L}\right) \qquad (9)$$

$$\Psi_{nm}(y_s z_s) = \cos(n\pi y_s)\cos\left(\frac{m\pi z_s}{L}\right) \qquad (10)$$

$$\alpha_{nm} = 1 \text{ when } \left(\frac{n\pi c}{\gamma\omega}\right)^2 + \left(\frac{m\pi c}{\gamma L\omega}\right)^2 \leq 1 \qquad (11)$$

$$\alpha_{nm} = +\,i \text{ when } \left(\frac{n\pi c}{\gamma\omega}\right)^2 + \left(\frac{m\pi c}{\gamma L\omega}\right)^2 > 1 \qquad (12)$$

$$\gamma^2 = \frac{1}{1 - M^2} \qquad (13)$$

$$N_y = \text{integer}_1\left(\frac{\gamma\omega}{\pi c}\right) \qquad (14)$$

$$N_z = \text{integer}\left(\frac{\gamma L\omega}{\pi c}\right) \tag{15}$$

$$\beta_n = 1 \qquad n = 0 \qquad \beta_n = \frac{1}{2} \qquad n > 0 \tag{16}$$

$$\beta_m = 1 \qquad m = 0 \qquad \beta_m = \frac{1}{2} \qquad m > 0 \tag{17}$$

$$\text{sgn}(x - x_s) = \frac{x - x_s}{|x - x_s|} \tag{18}$$

Details of the derivation are given in Appendix A.

Equation (6) describes the acoustic pressure in the duct for a harmonic ($e^{i\omega t} = e^{i2\pi f^* t}$) source of strength Q_o at position x_s, y_s, z_s. As seen in Eqs. (6), (11), and (12), the pressure is composed of a finite number of propagating acoustic modes ($\alpha_{nm} = 1$) and an infinite number of nonpropagating modes (evanescent, $\alpha_{nm} = i$). At sufficient distance from the source, the evanescent modes may generally be ignored. For this particular analysis, approximately five components of evanescent modes are used in the numerical calculations.

Also, as seen in Eqs. (6) and (8) for a given geometry, Mach number, and driving frequency $f^*(c = c^*/H^*f^*)$, K_{nm} will go to zero and P will approach infinity (resonance). Figure 3 shows experimental data (13) taken in the NASA Lewis acoustic duct laboratory for a compact combination of monopoles (small jet). For the resonance frequencies determined from Eq. (8), the pressure exhibits the predicted singular behavior; however, real fluid effects such as viscosity and nonlinearities limit the pressure jump. In addition, as seen by the center microphone curve, if the eigen-function $\Psi_{nm}(y,z)$ goes to zero, Ψ_{nm} will dominate over the singularity. This observation is used in the numerical calculations near a singularity. Also, no calculations are Performed directly on a singularity.

Finally, for a low frequency where only plane waves propagate, the $n = 0$ and $m = 0$ pressure mode from Eq. (6) is for x_s equal to zero

$$P(x,y,z,t) = \frac{Q_o}{2L} \frac{[1 - M\ \mathrm{sgn}(x)]}{(1 - M^2)} \exp\left[\frac{i\omega x\ \mathrm{sgn}(x)}{c(1 - M^2)}\right] e^{-i\omega t} \tag{19}$$

which is the classic plane wave propagation equation. The convective wave amplification jump at x equals zero comes directly from the M sgn (x) term.

Free Field Mathematical Model

The free field pressure solution for a moving (M_s) monopole source is given by Goldstein (11) in Eq. (1.111) in terms of an effective radius Re defined by Eq. (1.106). In terms of the x,y,z,t coordinate system of Fig. 2, the free field pressure can be expressed for a fixed source in a moving fluid ($M = -M_s$)

$$P(x,y,z,t) = \frac{Q_o\, e^{-i\omega t}}{4\pi Re(1 + M\cos\theta)^2}\left[\frac{-i\omega}{c} - \frac{M(\cos\theta + M)}{Re(1 + M\cos\theta)}\right] e^{i\omega Re/c} \tag{20}$$

$$Re = \frac{-M(x - x_s) + \sqrt{(x - x_s)^2 + (1 - M^2)r_s^2}}{1 - M^2} \tag{21}$$

$$\cos\theta + M = \frac{(x - x_s)}{Re} \tag{22}$$

$$1 + M\cos\theta = \sqrt{\frac{(x - x_s)^2 + (1 - M^2)r_s^2}{Re}} \tag{23}$$

$$r_s^2 = (y - y_s)^2 + (z - z_s)^2 \tag{24}$$

Equations (21) and (24) can be determined by reducing the general vector equation in Goldstein; however, these equations are explicitly developed by Morse and Ingard ((12), pp. 718-719).

Plane Wall Mathematical Model

The solution for a monopole adjacent to an infinite flat plane can be obtained directly from Eq. (20) by combining with a mirrored image source ((11), p. 62) of equal magnitude at location $- y_s$.

NUMERICAL RESULTS

In the calculations to follow, the analytical equations of the past sections will be used to determine tunnel resonance, tunnel frequency response, source directionality, modal energy content, tunnel alterations, and dipole response. The flow Mach number is taken to be 0.8 in all calculations to be presented. In the pressure response plots to follow, the absolute value of the pressure squared is plotted in log coordinates in the form

$$10 \log (P^2 + 1) \tag{25}$$

The source strength Q_0 in Eqs. (6) and (19) was arbitrarily chosen as 8.1 such that the $10 \log P^2$ had a value in the range of 30 to 70. The 1 in Eq. (25) was added to prevent negative value of the log at low frequencies. For all practical frequencies

$$10 \log (P^2 + 1) \approx 10 \log P^2 \tag{26}$$

Duct Resonance Frequencies

The resonance frequencies of the 8 by 6 wind tunnel were calculated from Eqs. (4) and (8) for various n and m modal numbers when K_{nm} is set to zero. The results of these calculations are displayed in Fig. 4, where a solid black line represents a duct resonance frequency. Below a frequency of 100 Hz discrete resonance values can be seen. The first resonance frequency occurs at 40 Hz. However, above 100 Hz the resonance frequencies become very dense and the individual modes are not distinguishable.

Figure 5 zooms in on the narrow band of frequencies about 1000 Hz where many experiments were conducted (1-5). Since the modes are dense, it would be difficult to not excite many adjacent modes with turboprop noise. The BPF

(Blade Passing Frequency) tone would not be narrow enough to avoid the duct resonances of Fig. 5.

Spectral Response

The spectral response of a monopole located in the center of the 8 by 6 wind tunnel ($x_s = 0$, $y_s = 0.5$, $z_s = 0.375$) is shown in Fig. 6. The response is measured at a position in the corner of the tunnel ($x = 0.5$, $y = 0$, $z = 0$), where all the duct modes are present and cut-off modes have a chance to decay. Recall the discussion of Fig. 3, by placing a microphone in a corner all the resonance modes will be observed. In the frequency range of Fig. 6, 1114 duct resonance values occur.

In Fig. 6, the response of the same strength monopole in the free field and adjacent to an infinite flat plane are also shown. Clearly, the theoretical response in the duct of the monopole is considerably higher than in the free field. Figure 7 displays the same information in a narrow band about 1000 Hz. At low frequencies and certain key frequencies as seen in Fig. 6, the pressure response in the duct drops below the free field response. The $\Psi_{nm}(y_s,z_s)$ term in Eqs. (6) and (10) partly accounts for this drop. For the present example (Figs. 6 and 7), y_s is 0.5 and z_s/L is 0.375; consequently,

$$\Psi_{nm}(y_s,z_s) = \cos\left(\frac{n\pi}{2}\right)\cos\left(\frac{m\pi}{2}\right) \tag{27}$$

For all propagating modes when n or m is odd, the value of Ψ_{nm} will be identical to zero. As a result, the spectral response strongly depends on the position of the source.

Source Directionality

Figures 8 to 10 show directionality results for source frequencies of 40, 90, and 1000 Hz. In Fig. 8, at the frequency of 40 Hz only the plane wave propagates. Ahead of the source ($x_T < 0$) the flow raises the pressure level

to nearly 30 while the pressure level trailing the source falls to about 10. Thus, a convective amplification of about 20 dB is seen. The pressure variation in the vicinity of the source is due solely to cut-off modes.

For the calculation displaced in Fig. 9, four higher order propagating modes exist at a slightly higher driving frequency of 90 Hz. The pressure near $x = 0$ is only a rough approximation in this range. Figure 10 displays similar results for a multimodal 1000 Hz source.

Similar to the propeller in a wind tunnel reported by Eversman and Baumeister (10) discussed earlier, for side line angles less than 45° or greater than 135° the similarity between duct directivity and free field can not be expected. In the free field, the pressure falls off as one over r while in the duct the propagating mode remains at constant amplitude.

Modal Amplitudes

For a 1000 Hz source, Fig. 11 displays the modal amplitudes as a function of their cut-off frequency. As discussed in the introduction, this closed form analysis was to be used to verify three-dimensional numerical approaches to the noise source problem which could handle the added complications of soft walls and variable area sheared flows. However, the use of conventional finite difference or finite element theories would be difficult because the modal amplitudes increase with frequency. Resolution of the near cut-off modes would require a prohibitively large number of transverse grid points or elements to resolve the harmonic pressure oscillations associated with the high cut off frequencies.

Tunnel Alterations

As shown in Fig. 1, the wind tunnel is often modified by the addition of wall plates or wings, which can change the reverberation characteristics of a tunnel. Figure 12 shows the effect of lowering the tunnel wall 0.1 and 0.2 dimensional increments. As seen in Fig. 12, the average directionality is

similar although the level shifts on average by as much as 10 downstream of the source.

Dipole Response

A propeller, as considered in Ref. 10, has its major noise lobe pointed downstream at an oblique angle and a small residual component pointed upstream. As suggested by Dittmar (9). the strong axial directivity of the propeller noise source could reduce reverberation effects in the vicinity of the source. The monopole just discussed, however, is an omnidirectional source. To eliminate the upstream component of the monopole, a dipole was chosen with the alignment shown in Fig. 13. In contrast to the monopole, a dipole noise source has strong directionality depending on its orientation. In the case shown in Fig. 13, the pressure lobes are directed toward the side walls, and in principle, could be swept downstream.

The pressure response of a dipole in a tunnel was modeled as two point harmonic monopoles 180° out of phase separated by a small distance 2h. The strength of a free field monopole Q_0 to simulate a dipole of strength D, can be expressed as ((14), p. 572) Eq. (13.482))

$$Q_0 = \frac{D_0}{2h} \tag{28}$$

Figure 13 displays the frequency response of this dipole in the narrow band about 1000 Hz. As seen in this spectral plot, many of the harmonic peaks of Fig. 7 have been cancelled. Figure 14 shows the directionality of a source at 1000 Hz. In the vicinity of the source, the dipoles average pressure response roughly follows the response of the dipole in the free field. Again, as with the propeller analysis of Ref. 10, for side line angles less than 45° or greater than 135° similarity between duct directivity and free field could not be expected. The amplitudes of the tunnel and free field response are now within 10. In an actual transonic tunnel, as shown in Fig. 1, the walls have

holes and will therefore appear soft in an acoustic sense. Consequently, the difference between the free field and tunnel results shown in Fig. 14 would be the maximum possible. In the actual tunnel, soft wall absorption will occur and the tunnel and free field values will approach each other more closely.

CONCLUDING REMARKS

Analytical solutions for the three-dimensional inhomogeneous wave equation with flow in a hard wall wind tunnel and in the free field are presented for a monopole noise source. Numerical calculation for the modal content, spectral response, and directivity for both monopole and dipole sources are presented. In the frequency range of practical importance to turboprop response, some important features of the free field directivity can be approximated in a hard wall wind tunnel with flow if the major lobe of the noise source is not directed upstream. However, for a omnidirectional source, such as a monopole, the wind tunnel and free field response will not be comparable.

APPENDIX A

Wind Tunnel Solution

As shown in the body of the report, for a monopole source, the wave Eq. (1) can be written as

$$(1 - M^2)\frac{\partial^2\varphi}{\partial x_f^2} + \frac{\partial^2\varphi}{\partial y_f^2} + \frac{\partial^2\varphi}{\partial z_f^2} - \frac{2M}{c}\frac{\partial^2\varphi}{\partial x_f \partial t} - \frac{1}{c^2}\frac{\partial^2\varphi}{\partial t_f^2}$$

$$= q_o(t_f)\delta(x_f)\delta(y_f - y_s)\delta(z_f - z_s) \qquad (A1)$$

The solution to Eq. (A1) can be more conveniently obtained by rewriting Eq. (A1) in a Gallilean (x_g, y_g, z_g, t_g) system moving with the flow. Therefore, assume

$$x_f = x_g + Ut_g = x_g + CMt_g \qquad x_g = x_f - Ut_f \qquad (A2)$$

$$y_f = y_g, \qquad z_f = z_g, \qquad t_f = t_g \qquad (A3\text{-}5)$$

As discussed by Morse and Ingard ((12), p. 701), the space derivatives are invariant under this transformation; however, the time derivatives become

$$\frac{\partial\varphi(x_g, t_g)}{\partial t_f} = \frac{\partial\varphi}{\partial t_g}\frac{\partial t_g}{\partial t_f} + \frac{\partial\varphi}{\partial x_g}\frac{\partial x_g}{\partial t_f} = \frac{\partial\varphi}{\partial t_g} - U\frac{\partial\varphi}{\partial x_g} \qquad (A6)$$

$$\frac{\partial^2\varphi}{\partial t_f^2} = \frac{\partial^2\varphi}{\partial t_g^2} - 2U\frac{\partial^2\varphi}{\partial t_g \partial x_g} + U^2\frac{\partial^2\varphi}{\partial x_g^2} \qquad (A7)$$

where U equals CM as defined in the list of symbols. Thus, the wave Eq. (A1) becomes

$$\frac{\partial^2\varphi}{\partial x_g^2} + \frac{\partial^2\varphi}{\partial y_g^2} + \frac{\partial^2\varphi}{\partial z_g^2} - \frac{1}{c^2}\frac{\partial^2\varphi}{\partial t_g^2} = q_o(t_g)\delta(x + Ut_g)\delta(y_g - y_s)\delta(z_g - z_s) \qquad (A8)$$

Finally, to match the general form of equations as used by Goldstein ((10), p. 45) and Morse and Ingard ((12), p. 721) which employ moving source, let

$$U = -V \tag{A9}$$

Therefore Eq. (12) becomes

$$\frac{\partial^2\varphi}{\partial x_g^2} + \frac{\partial^2\varphi}{\partial y_g^2} + \frac{\partial^2\varphi}{\partial z_g^2} - \frac{1}{c^2}\frac{\partial^2\varphi}{\partial t_g^2} = q_o(t_g)\delta(x - Vt_g)\delta(y_g - y_s)\delta(z_g - z_s) \tag{A10}$$

To obtain a solution of Eq. (A10), Morse and Ingard ((12), p. 722) suggest employing a Lorentz transformation of the form

$$x' = \gamma(x_g - Vt_g) \qquad y' = y_g \qquad z' = z_g \tag{A11-13}$$

$$t' = \gamma\left(t_g - \frac{V}{c^2}x_g\right) \tag{A14}$$

or combining Eqs. (A11) and (A14)

$$t_g = \gamma\left(t' + \frac{V}{c^2}x'\right) \tag{A15}$$

where

$$\gamma = \frac{1}{\sqrt{1 - M^2}} \tag{A16}$$

$$M^2 = \left(\frac{V}{C}\right)^2 = \left(\frac{U}{C}\right)^2 \tag{A17}$$

In contrast to the Galilean transform, both space and time are involved in the transform. Noting that $\varphi[x_g(x',t'),t_g(x',t')]$

$$\frac{\partial\varphi(x',t')}{\partial x_g} = \frac{\partial\varphi}{\partial x'}\frac{\partial x'}{\partial x_g} + \frac{\partial\varphi}{\partial t'}\frac{\partial t'}{\partial x_g} = \gamma\frac{\partial\varphi}{\partial x'} - \gamma\frac{V}{c^2}\frac{\partial\varphi}{\partial t'} \tag{A18}$$

$$\frac{\partial^2\varphi}{\partial x_g^2} = \gamma^2\frac{\partial^2\varphi}{\partial x'^2} - 2\frac{\gamma^2 V}{c^2}\frac{\partial^2\varphi}{\partial x'\partial t'} + \gamma^2\frac{V^2}{c^4}\frac{\partial\varphi}{\partial t'} \tag{A19}$$

$$\frac{\partial\varphi(x',t')}{\partial t_g} = \frac{\partial\varphi}{\partial t'}\frac{\partial t'}{\partial t_g} + \frac{\partial\varphi}{\partial x'}\frac{\partial x'}{\partial t_g} = \gamma\frac{\partial\varphi}{\partial t'} - \gamma V\frac{\partial\varphi}{\partial x'} \tag{A20}$$

$$\frac{\partial^2\varphi}{\partial t_g^2} = \gamma^2\frac{\partial^2\varphi}{\partial t'^2} - 2\gamma^2 V\frac{\partial^2\varphi}{\partial t'\partial x'} + \gamma^2 V^2\frac{\partial^2\varphi}{\partial x'^2} \tag{A21}$$

$$\delta(x_g - Vt_g) = \delta\left(\frac{x'}{\gamma}\right) \tag{A22}$$

and using Eq. (A15)

$$q_0(t_g) = q_0\left(\gamma\left[t' + \frac{V}{c^2}x'\right]\right) \tag{A23}$$

Thus, the wave equation in the Lorentz system becomes

$$\frac{\partial^2\varphi}{\partial x'^2} + \frac{\partial^2\varphi}{\partial y'^2} + \frac{\partial^2\varphi}{\partial z'^2} - \frac{1}{c^2}\frac{\partial^2\varphi}{\partial t'^2} = \gamma q_0(\gamma t')\delta(x')\delta(y' - y'_s)\delta(z' - z'_s) \tag{A24}$$

The $V/c^2\ x'$ term in q_0 was dropped because the right hand side of Eq. (A24) has a nonzero value only when x' equals zero because of $\delta(x')$.

Finally, the wave equation reduces to an equivalent stationary system when it is assumed

$$x' = x''/\gamma \qquad x'' = \gamma x' \tag{A25}$$

$$y'' = y'/\gamma \qquad y'' = \gamma y' \tag{A26}$$

$$z' = z''/\gamma \qquad z'' = \gamma z' \tag{A27}$$

$$t' = t''/\gamma \qquad t'' = \gamma t' \tag{A28}$$

As a result,

$$\frac{\partial^2\varphi}{\partial x'^2} = \gamma^2\frac{\partial^2\varphi}{\partial x''^2} \text{ (same for y, z, and t)} \tag{A29}$$

also

$$1 \equiv \int_{-\infty}^{\infty}\delta(x')dx' = \int_{-\infty}^{\infty}\delta\left(\frac{x''}{\gamma}\right)\frac{1}{\gamma}dx'' = \int_{-\infty}^{\infty}\delta(x'')dx'' \equiv 1 \tag{A30}$$

therefore,

$$\frac{1}{\gamma}\delta\left(\frac{x''}{\gamma}\right) = \delta(x'') \tag{A31}$$

and

$$\delta\left(\frac{x''}{\gamma}\right)\delta\left(\frac{y''}{\gamma}\right)\delta\left(\frac{z''}{\gamma}\right) = \gamma^3\delta(x'')\delta(y'')\delta(z'') \tag{A32}$$

Thus, the wave equation in stationary coordinates becomes

$$\frac{\partial^2\varphi}{\partial x''^2} + \frac{\partial^2\varphi}{\partial y''^2} + \frac{\partial^2\varphi}{\partial z''^2} - \frac{1}{c^2}\frac{\partial^2\varphi}{\partial t''^2} = \gamma^2 q_0(t'')\delta(x'')\delta(y'' - y_s'')\delta(z'' - z_s'') \qquad \text{(A33)}$$

Lets now assume the driving source to be harmonic and of the form

$$\varphi(x'',y'',t'') = \Phi(x'',y'',z'')e^{-i\omega t''} \qquad \text{and} \qquad q_0(t) = Q_0\, e^{-i\omega t''} \qquad \text{(A34)}$$

Consequently, the governing wave equation becomes

$$\frac{\partial^2\Phi}{\partial x''^2} + \frac{\partial^2\Phi}{\partial y''^2} + \frac{\partial^2\Phi}{\partial z''^2} + k^2\Phi = \gamma^2 Q_0\, \delta(x'')\delta(y'')\delta(z'') \qquad \text{(A35)}$$

where k equals ω/c

The solution to a form of Eq. (A35) is considered by Morse and Ingard ((12), p. 500). Because of certain differences, some details of the solution to Eq. (A35) are now presented. Assuming

$$\Phi = X(x'')Y(y'')Z(z'')$$

and substitution into homogeneous form of Eq. (A35)

$$\frac{1}{Y}\frac{\partial^2 Y}{\partial y''^2} + \frac{1}{Z}\frac{\partial^2 Z}{\partial z''^2} + k^2 = -\frac{1}{X}\frac{\partial^2 X}{\partial x''^2} = +k_x^2$$

where k_x is the separation constant. The solution for $X(x'')$ yield

$$X = c_1\, e^{-ik_x x''} + c_2\, e^{ik_x x''} \qquad \text{(A36)}$$

For the imposed exit condition of no reflection at + and - infinity,

$$X = c_+\, e^{+ik_x x''} \qquad x'' > o \qquad \text{(A37)}$$

$$X = c_-\, e^{-ik_x x''} \qquad x'' < o \qquad \text{(A38)}$$

Similarly

$$\frac{1}{Z}\frac{\partial^2 Z}{\partial z''^2} + k^2 - k_x^2 = -\frac{1}{Y}\frac{\partial^2 Y}{\partial y''^2} = k_y^2 \tag{A39}$$

which yields

$$Y = A_1 \cos k_y y'' + A_2 \sin k_y y'' \tag{A40}$$

and

$$Z = B_1 \cos k_z z'' + B_2 \sin k_z z'' \quad z'' \tag{A41}$$

where

$$k_z^2 = k^2 - k_x^2 - k_y^2 \tag{A42}$$

The transverse boundary condition at the hard wall requires the acoustic velocities to be zero. According to Eq. (2) at $y_t = y'' = o$ and $z_t = z'' = 0$, $\partial y/\partial y'' = 0$ and $\partial z/\partial z'' = 0$, thus

$$\Phi = C_+ \cos k_y y'' \cos k_z z'' e^{+ik_x x''} \qquad x'' > 0 \tag{A43}$$

$$\Phi = C_- \cos k_y y'' \cos k_z z'' e^{+ik_x x''} \qquad x'' < 0 \tag{A44}$$

The second boundary condition requires the velocity to be zero at $y_t = 1$ and $z_t = L$ as shown in Fig. 2. In the coordinate transform, this requires that the velocity be zero at $y'' = \gamma$ and $z'' = \gamma L$. Consequently, the eigen-values k_y and k_z are such that Eqs. (A43) and (A44) become

$$\Phi_{nm}(x'',y'',z'') = C_+ \cos \frac{n\pi}{\gamma} y'' \cos \frac{m\pi}{\gamma L} z'' e^{+ik_x x''} \qquad x'' > 0 \tag{A45}$$

$$= C_- \cos \frac{n\pi}{\gamma} y'' \cos \frac{m\pi}{\gamma L} z'' e^{-ik_x x''} \qquad x'' < 0 \tag{A46}$$

where

$$k_x = \left(\frac{\omega}{c}\right)\sqrt{1 - \left(\frac{n\pi c}{\gamma\omega}\right)^2 - \left(\frac{m\pi c}{\gamma\omega L}\right)^2} \tag{A47}$$

Equations (A45) and (A46) represent the separate homogeneous solution to the wave Eq. (A35) in the negative and positive domain of the spatial variable x. What remains is to determine the constants C_+ and C_- from the nonhomogenous term on the right hand side of Eq. (A35).

For the no flow case considered here, the x momentum equation can be integrated between $x = -\epsilon$ and $x = +\epsilon$. As ϵ goes to zero, it is seen that both the pressure and the velocity potential are continuous across a monopole. Consequently C_+ and C_- are equal in magnitude and Eqs. (A45) and (A46) become

$$\Phi_{nm}(x'',y'',z'') = C_{nm} \cos \frac{n\pi}{\gamma} y'' \cos \frac{m\pi}{\gamma L} z'' \, e^{ik_x|x''|} \tag{A48}$$

In contrast, a dipole would have continuous velocity and a discontinuous pressure and velocity potential.

The last step remaining is to determine the constant C_{nm}. For simplicity, let

$$\psi_{nm} = C_{nm} \, e^{ik_x|x''|} \tag{A49}$$

Thus,

$$\Phi = \sum_{n=0}^{\infty} \sum_{m=0}^{\infty} \psi_{nm} \cos \frac{n\pi}{\gamma} y'' \cos \frac{m\pi}{\gamma L} z'' \tag{A50}$$

Substituting Eq. (A50) into the wave Eq. (A33), multiplying both sides of the equation by $\cos a\pi y/\gamma \cos b\pi z/\gamma L$ and integrating yields for any value of n or m

$$\int_0^{\gamma L} \int_0^{\gamma} \left\{ \frac{\partial \psi_{nm}^2}{\partial x''^2} + \left[k^2 - \left(\frac{n\pi}{\gamma}\right)^2 - \left(\frac{m\pi}{\gamma L}\right)^2 \right] \psi_{nm} \right\} \cos \frac{n\pi y''}{\gamma} \cos \frac{m\pi z''}{\gamma L} \cos \frac{a\pi y''}{\gamma} \cos \frac{b\pi z''}{\gamma L} \, dy''dz''$$

$$= \int_0^{\gamma L} \int_0^{\gamma} \gamma^2 Q \, \delta(x'')\delta(y'' - y_s'')\delta(z'' - z_s'') \cos \frac{a\pi y''}{\gamma} \cos \frac{b\pi z''}{\gamma L} \, dy''dz'' \tag{A51}$$

The above integration will remove the delta function from the differential equation, because for any function g

$$\int \delta(y'' - y_s'')g(y'')dy = g(y_s') \tag{A52}$$

Finally, because of the orthogonality of the cosine, Eq. (A51) becomes

$$\frac{\partial^2 \psi_{nm}}{\partial x''} + \left[k^2 - \left(\frac{n\pi}{\gamma}\right)^2 - \left(\frac{n\pi}{\gamma L}\right)^2\right] \psi_{nm} = \frac{Q_o\, \delta(x'') \cos \frac{n\pi}{\gamma} y_s'' \cos \frac{m\pi}{\gamma L} z_s''}{L\, \beta_n \beta_m} \tag{A53}$$

where

$$\beta_n = 1 \qquad n = o \qquad \beta_n = \frac{1}{2} \qquad n > o \tag{A54}$$

$$\beta_m = 1 \qquad m = o \qquad \beta_m = \frac{1}{2} \qquad m > o \tag{A55}$$

The multiple values of β_n are a consequence of the properties of the integral of $\cos^2 ny''$.

Finally, substituting Eq. (A49) back into Eq. (A53), integrating both sides of the equation between $x = -\varepsilon$ and $x = +\varepsilon$ and letting ε approach zero (see (12). p. 133 for details) yields

$$C_{nm} = -\frac{i\, Q_o \cos \frac{n\pi}{\gamma} y_s'' \cos \frac{m\pi}{\gamma L} z_s''}{2\, k_x L \beta_n \beta_m} \tag{A56}$$

For ease of calculation let k_x in Eq. (A47) be rewritten as

$$k_x = \frac{\omega}{c} K_{nm} \alpha_{nm} \tag{A57}$$

as defined by Eqs. (8), (11), and (12) in the body of the report. Thus,

$$\Phi(x'',y'',z'') = \sum_{n=0}^{\infty} \sum_{m=0}^{\infty} - \frac{iQ_o \left[\cos \frac{n\pi}{\gamma} y_s'' \cos \frac{m\pi}{\gamma L} z_s''\right]}{2\omega \alpha_{nm} K_{nm} L \beta_n \beta_m} \cos \frac{n\pi y''}{\gamma} \cos \frac{m\pi z''}{\gamma L} e^{i\alpha_{nm} K_{nm} \frac{\omega}{c} |x''|} \tag{A58}$$

Equation (A58) represents the potential in the stationary system. This equation must be transformed back into the tunnel coordinate system in Fig. 2. First, the equation is transformed back into the Lorentz's system by substituting Eqs. (A25) to (A28) into Eq. (A58) to yield

$$\Phi(x',y',z') = \frac{-iQ_o c}{2L\omega} \sum_{n=0}^{\infty}\sum_{m=0}^{\infty} \frac{\cos n\pi y_s' \cos \frac{m\pi z_s'}{L} \cos n\pi y' \cos \frac{m\pi z'}{L}}{\beta_n \beta_m K_{nm} \alpha_{nm}}$$

$$\times e^{i\frac{\omega}{c}\gamma|x'|\alpha_{nm}K_{nm}} \qquad \text{(A59)}$$

where Eq. (A34)

$$\varphi(x',y',z',t') = \Phi(x',y',z')e^{-i\omega\gamma t'} \qquad \text{(A60)}$$

Next, Eqs. (A59) and (A60) must be transformed to the Gallilean (x_g,y_g,z_g,t_g) system. Multiplying Eq. (A14) by γ

$$\gamma t' = \gamma^2 t_g - \frac{V}{c^2} x_g \gamma^2 \qquad \text{(A61)}$$

and noting that

$$t_g = t_g(1 - M^2) + M^2 t_g = \frac{t_g}{\gamma^2} + M^2 t_g = \frac{t_g}{\gamma^2} + \frac{V^2}{c^2} t_g \qquad \text{(A62)}$$

then replacing t_g in Eq. (A61) with Eq. (A62)

$$\gamma t' = t_g - \frac{\gamma^2 V}{c^2}(x_g - Vt_g) \qquad \text{(A63)}$$

Substituting Eqs. (A11), (A12), (A3), (A63), and (A9) into Eqs. (A59) and (A60) yields

$$\Phi(x_g,y_g,z_g) = \frac{-iQ_o c}{2L\omega} \sum_{n=0}^{\infty}\sum_{m=0}^{\infty} \frac{\Psi_{nm}(y_s,z_s)\Psi_{nm}(y_g,z_g)}{\beta_n \beta_m K_{nm} \alpha_{nm}} e^{i\frac{\omega}{c}\alpha_{nm}K_{nm}\gamma|x_g + V_o t_g|} \qquad \text{(A64)}$$

$$\varphi(x_g,y_g,z_g,t_g) = \Phi(x_g,y_g,z_g)\, e^{-i\omega t_g}\, e^{i\omega\gamma^2 V/c^2\,(x_g + U_o t_g)} \tag{A65}$$

where

$$\Psi_{nm}(y_s,z_s) = \cos n\pi y_s \cos \frac{m\pi z_s}{L} \tag{A66}$$

$$\Psi_{nm}(y_g,z_g) = \cos n\pi y_g \cos \frac{m\pi z_g}{L} \tag{A67}$$

The sign of $(x + U_o t)$ in Eq. (A65) need not be considered because this will be removed in the next transform to tunnel coordinates.

Substituting Eqs. (A2) to (A5) into Eqs. (A64) and (A65) yields

$$\Phi(x_f,y_f,z_f) = -i\frac{Q_{oc}}{2L\omega} \sum_{n=0}^{\infty}\sum_{m=0}^{\infty} \frac{\Psi_{nm}(y_s,z_s)\Psi_{nm}(y_f,z_f)}{\beta_n\beta_m K_{nm}\alpha_{nm}}\, e^{i\frac{\omega}{c}\alpha_{nm}K_{nm}|x_f|} \tag{A68}$$

$$\varphi(x_f,y_f,z_f,t_f) = \Phi(x_f,y_f,z_f) e^{-i\omega t_f} e^{i\omega\gamma^2 V/c^2\, x_f} \tag{A69}$$

The Ψ terms have the same functional form. Combining Eqs. (A68) and (A69) and substituting into Eq. (3) in the body of the report yield for pressure

$$P(x_f,y_f,z_f,t_f) = \left\{ \frac{Q_o}{2L} \sum_{n=0}^{\infty}\sum_{m=0}^{\infty} \frac{\Psi_{nm}(y_f,z_f)\Psi_{nm}(y_s,z_s)}{\beta_n\beta_m\alpha_{nm}K_{xnm}} \times \gamma^2 \left[1 - M\,\alpha_{nm}K_{nm}\,\mathrm{sgn}\,(x_f)\right] \right.$$
$$\left. \times \exp\left[\frac{i\gamma^2\omega}{c}\left(\alpha_{nm}K_{nm}|x_f| - Mx_f\right)\right] \right\} e^{i\omega t_f} \tag{A70}$$

Note, in taking the spatial derivative of $e^{|x_f|}$

$$\frac{\partial}{\partial x} e^{A|x_f|} = \mathrm{sgn}\,(x_f) A\, e^{A|x|} \tag{A71}$$

where

$$\mathrm{sgn}(x_f) \equiv \frac{x_f}{|x_f|} \tag{A72}$$

as easily seen by rewriting two separate equations for $\exp A|x|$ for x greater than zero and x less than zero. Finally, we transform to the tunnel coordinate system, noting that

$$x = x_f + x_s \qquad x_f = x - x_s \tag{A73}$$

$$y = y_f, \qquad z = z_f, \qquad t = t_f \tag{A74-A76}$$

The resulting equation is Eq. (6) in the body of the report.

REFERENCES

1. Dittmar, J.H., Blaha, B.J., and Jeracki, R.J., "Tone Noise of Three Supersonic Helical Tip Speed Propellers in a Wind Tunnel at 0.8 Mach Number," NASA TM-79046 (1978).

2. Dittmar, J.H., Jeracki, R.J., and Blaha, B.J., "Tone Noise of Three Supersonic Helical Tip Speed Propellers in a Wind Tunnel," NASA TM-79167 (1979).

3. Dittmar, J.H., Jeracki, R.J., "Additional Noise Data on the SR-3 Propeller," NASA TM-81736 (1981).

4. Dittmar, J.H., Stefko, G.L., and Jeracki, R.J., "Noise of the 10-Bladed, 40° Swept SR-6 Propeller in a Wind Tunnel," NASA TM-82950 (1982).

5. Dittmar, J.H., Stefko, G.L., and Jeracki, R.J., "Noise of the 10-Bladed, 60° Swept SR-5 Propeller in a Wind Tunnel," NASA TM-83054 (1983).

6. Dittmar, J.H. and Jeracki, R.J., "Noise of the SR-3 Propeller Model at 2 and 4° Angle of Attack," NASA TM-82738 (1981).

7. Mackall, K.G., Lasagna. P.L., Walsh, K., and Dittmar, J.H., "In-Flight Acoustic Results from an Advanced-Design Propeller at Mach Numbers to 0.8," AIAA Paper No. 82-1120 (1982).

8. Dittmar, J.H. and Lasagna, P.L., "A Preliminary Comparison Between the SR-3 Propeller Noise in Flight and in a Wind Tunnel," NASA TM-82805 (1982).

9. Dittmar, J.H., "Why Credible Propeller Noise Measurements are Possible in the Acoustically Untreated NASA Lewis 8 by 6 Ft Wind Tunnel," J. Acoust. Soc. Am., vol. 75. no. 6, June 1984, pp. 1913-1914.

10. Eversman, W. and Baumeister, K.J., "Modeling of Wind Tunnel Wall Effects on the Radiation Characteristics of Acoustic Sources," AIAA Paper No. 84-2364 (1984).

11. Goldstein, M.E., "Aeroacoustics," McGraw-Hill, New York, 1976.

12. Morse, P.M. and Ingard, K.U., "Theoretical Acoustics," McGraw-Hill, New York, 1968.

13. Succi, G.P., Baumeister, K.J., and Ingard, K.U., "Interaction of a Turbulent-Jet Noise Source with Transverse Modes in a Rectangular Duct," NASA TP-1248, June 1978.

14. Reynolds, Douglas D., "Engineering Principles of Acoustics Noise and Vibration Control," Allyn and Bacon, Inc. (1981).

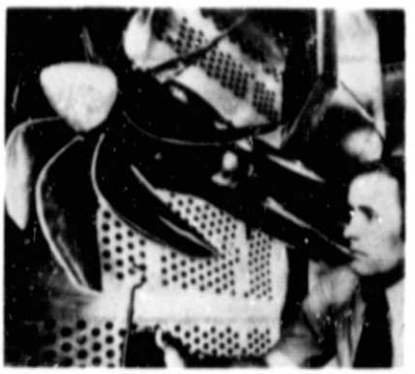

PROPELLER ALONE AND AT ANGLE ATTACK

INSTALLATION EFFECTS AND BLADE MOUNTED TRANSDUCERS

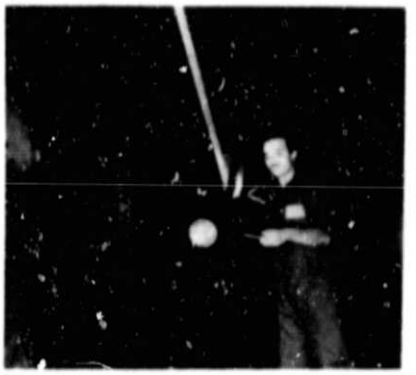

WING SHIELDING

BOUNDARY LAYER REFRACTION

Figure 1. - Advanced prop-fan instailations in NASA Lewis Research Center 8x6ft Transonic Wind Tunnel.

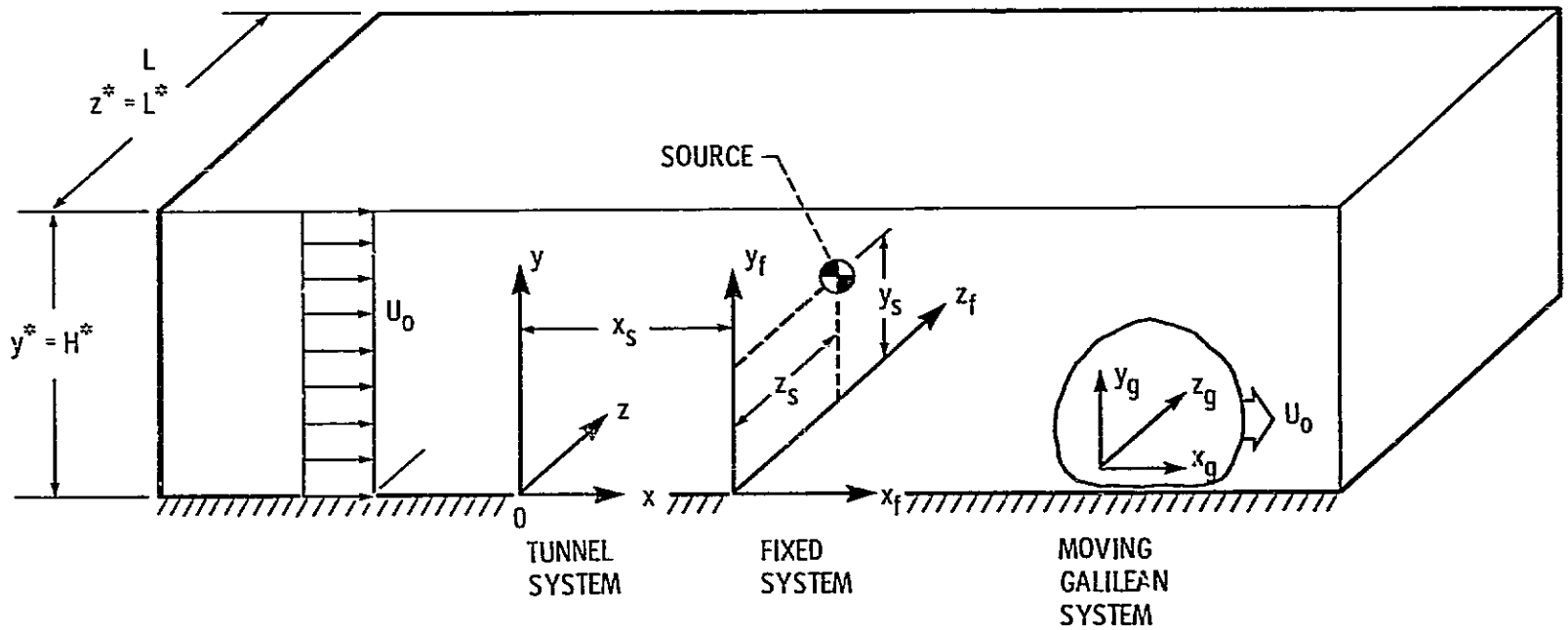

Figure 2. - Tunnel coordinate systems.

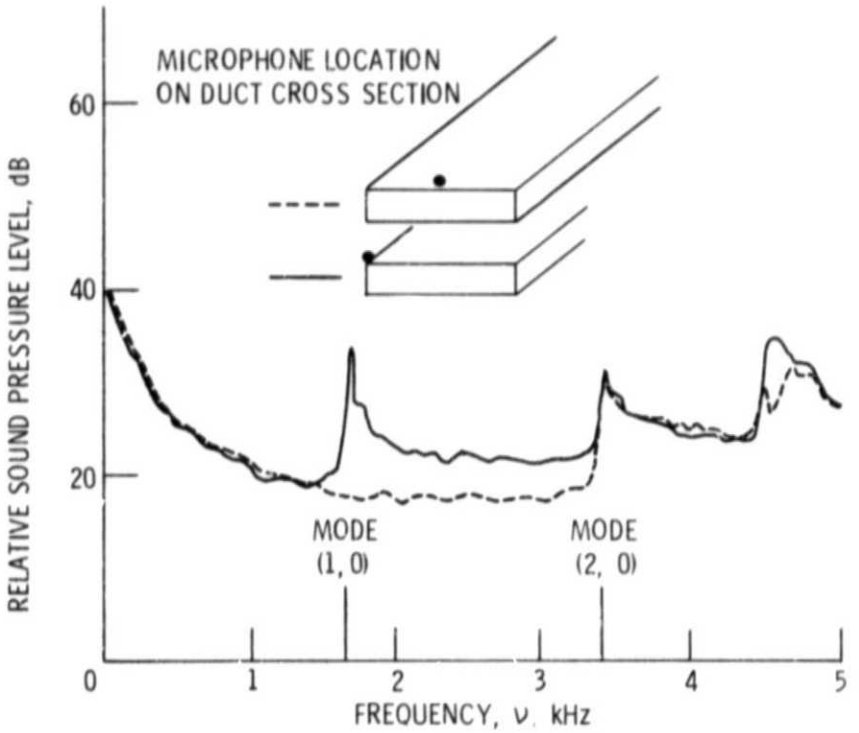

Figure 3. - Modal response of a small rectangular duct (ref. 13).

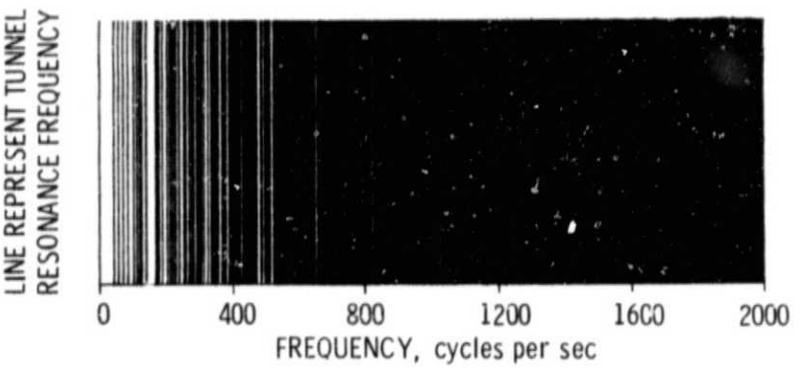

Figure 4. - Resource frequencies of the 8x6 ft wind tunnel.

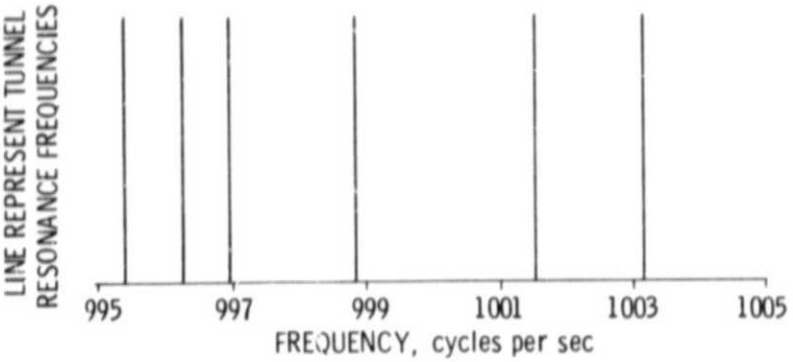

Figure 5. - Resonance frequencies of the 8x6 ft wind tunnel in a narrow band about 1000 cycles per sec.

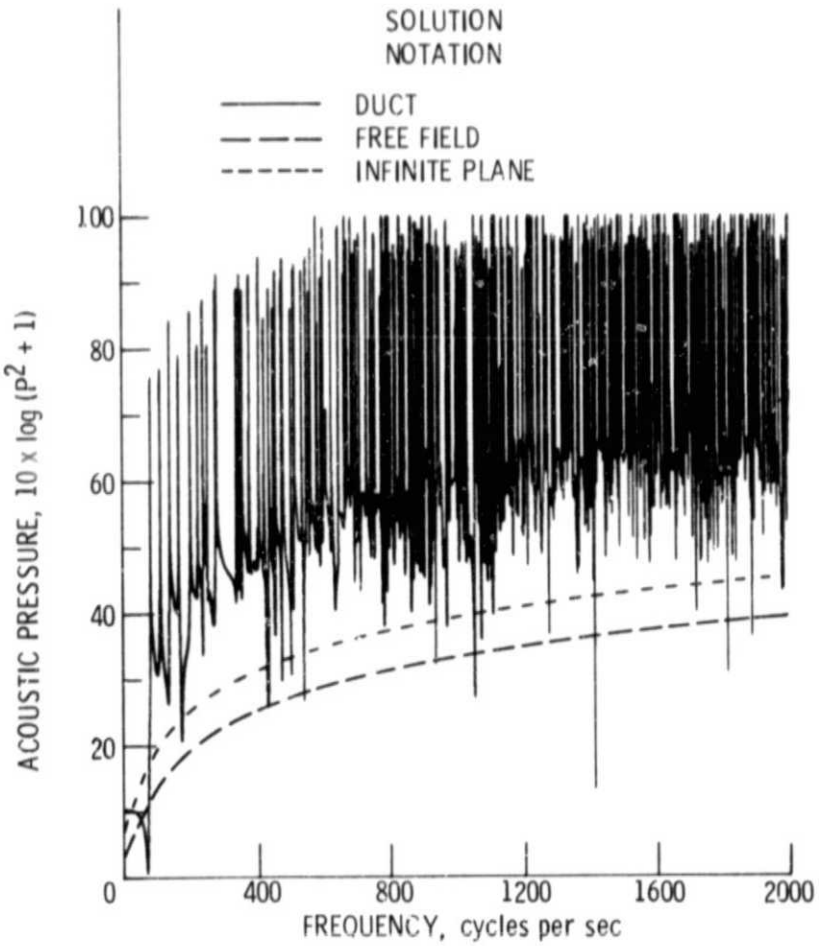

Figure 6. - Spectral response of a monopole located in the center of the tunnel ($x_S = 0$, $y_S = 0.5$, $z_S = 0.375$) at $x = 0.5$, $y = 0$, $z = 0$. ($Q = 8.1$, $M = 0.8$)

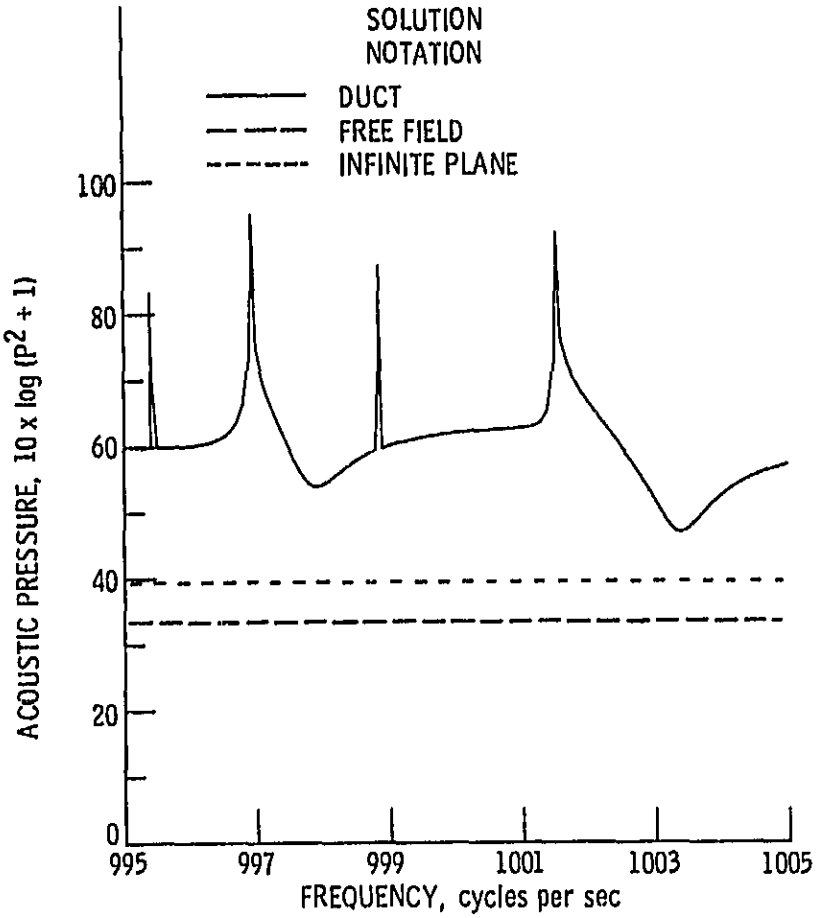

Figure 7. - Spectral response of a monopole of figure 6 in a narrow band about 1000 Hz.

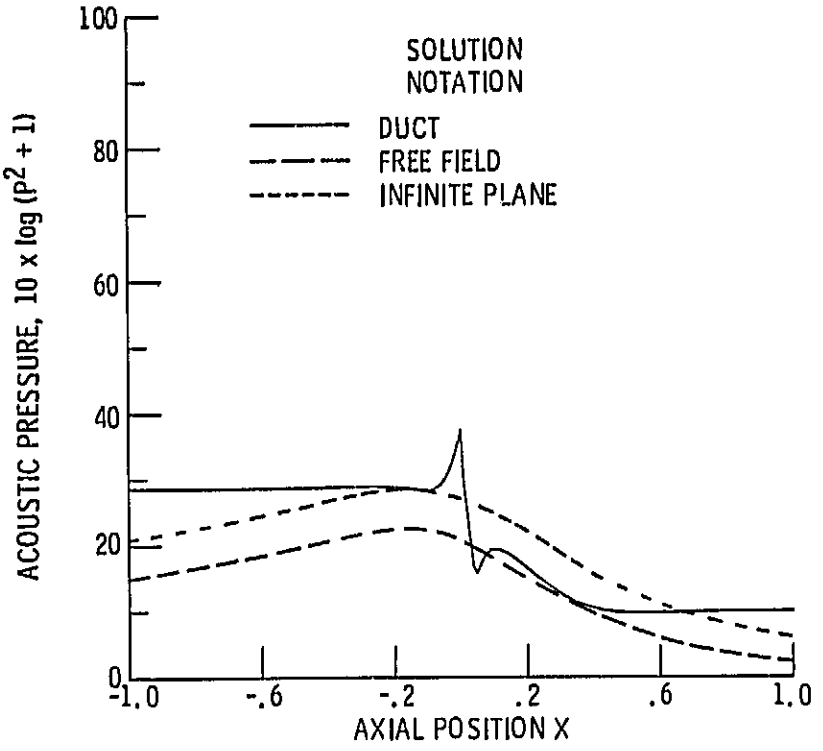

Figure 8. - Wall pressure response for a 40 Hz monopole ($y = 0$, $z = 0.375$, $x_s = 0$, $y_s = 0.5$, $z_s = 0.375$).

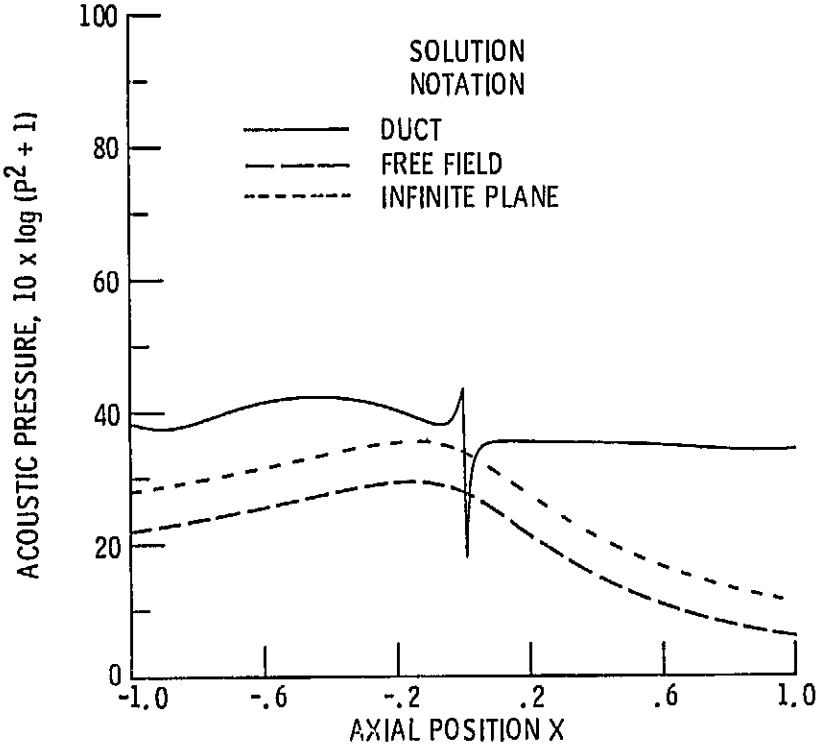

Figure 9. - Wall pressure response for a 90 Hz monopole ($y = 0$, $z = 0.375$, $x_s = 0$, $y_s = 0.5$, $z_s = 0.375$).

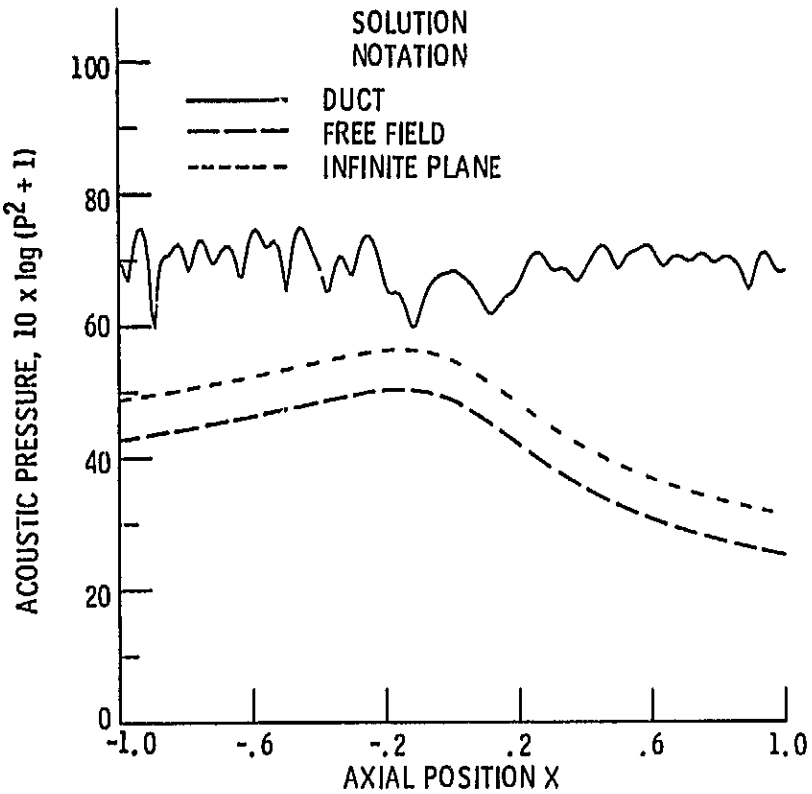

Figure 10. - Wall pressure response for a 1000 Hz monopole ($y = 0$, $z = 0.375$, $x_s = 0$, $y_s = 0.5$ and $z_s = 0.375$).

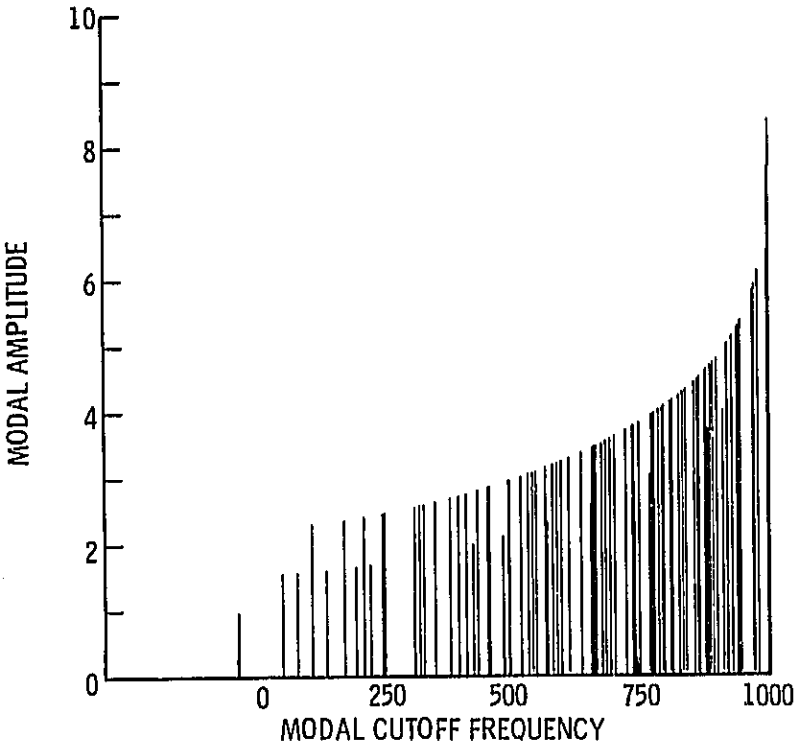

Figure 11. - Modal amplitude of propagating acoustic modes for 1000 Hz monopole source.

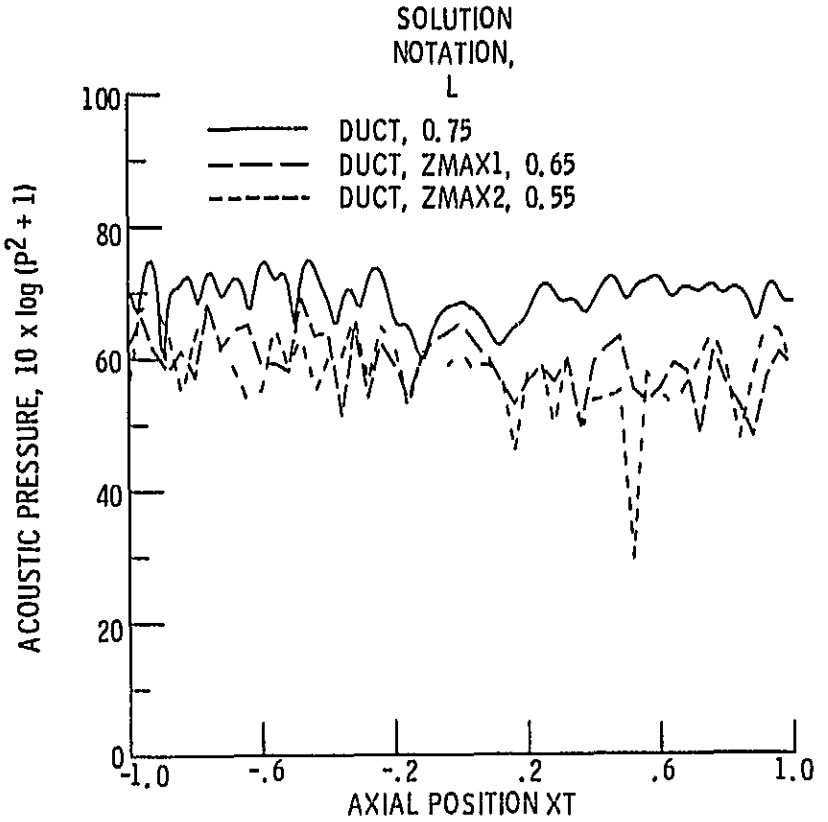

Figure 12. - Effect of tunnel alterations on directivity of 1000 Hz monopole source (x_s = 0.0, y_s = 0.5, z_s = 0.375, y = 0.0, z = 0.375).

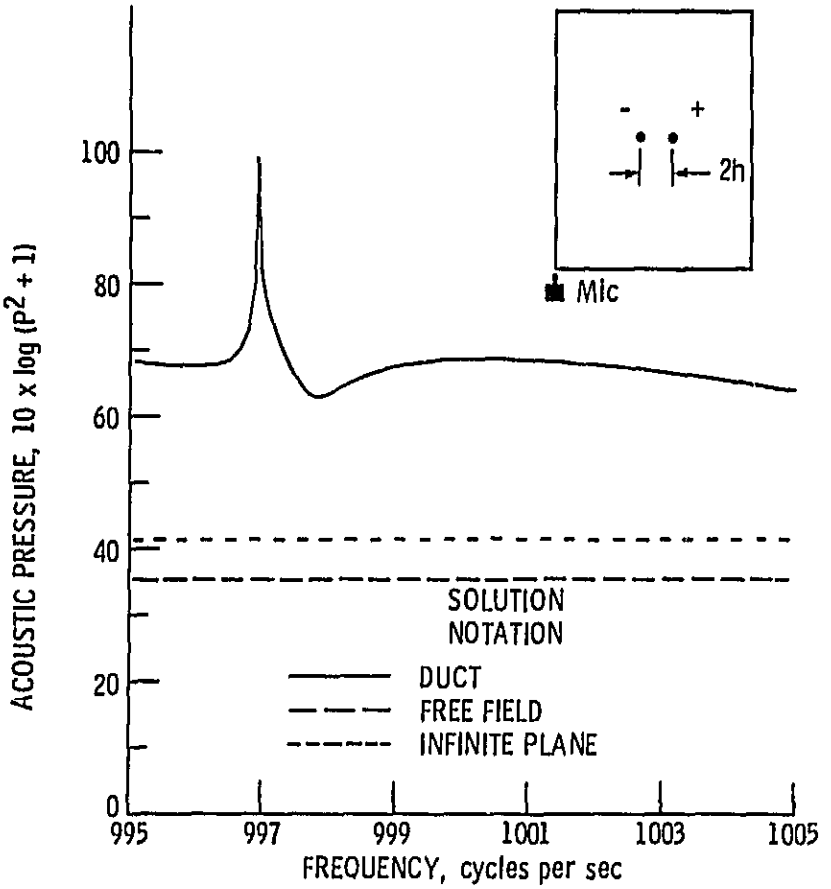

Figure 13. - Spectral response of a dipole in a narrow band about 1000 Hz (Q = 8.1, 2h = 0.05, x = 0.5, y = 0, z = 0, M = 0.8)

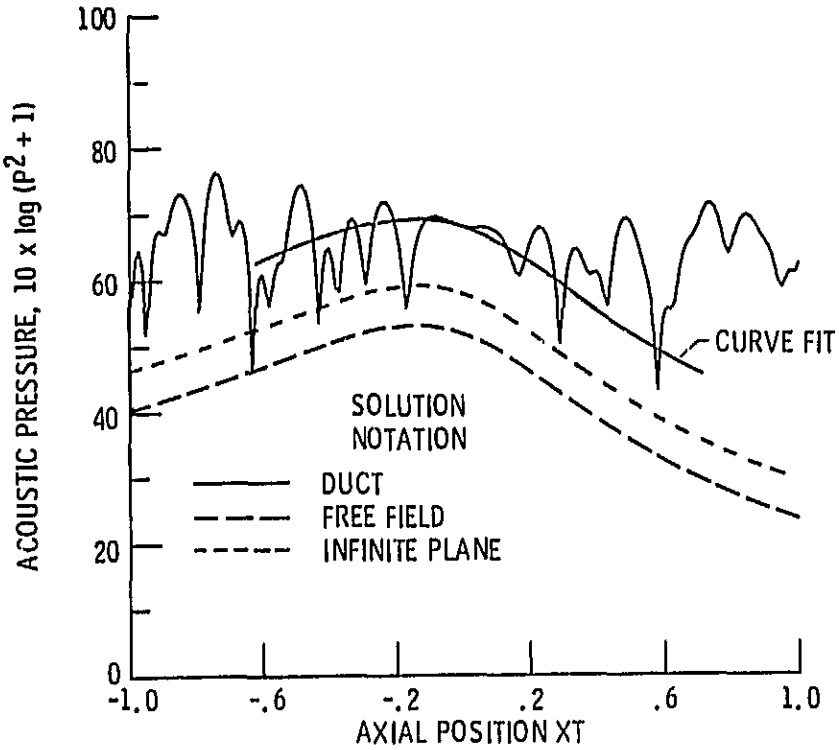

Figure 14. - Wall pressure response for a 1000 Hz dipole at y = 0 and z = 0 (x_s = 0, y_s = 0.5, z_s = 0.375, M = 0.8).

1. Report No.	2. Government Accession No.	3. Recipient's Catalog No.
NASA TM-87063		

4. Title and Subtitle	5. Report Date
Reverberation Effects on Directionality and Response of Stationary Monopole and Dipole Sources in a Wind Tunnel	6. Performing Organization Code: 505-40-90

7. Author(s)	8. Performing Organization Report No.
Kenneth J. Baumeister	E-2432
	10. Work Unit No.

9. Performing Organization Name and Address	11. Contract or Grant No.
National Aeronautics and Space Administration Lewis Research Center Cleveland, Ohio 44135	13. Type of Report and Period Covered: Technical Memorandum

12. Sponsoring Agency Name and Address	14. Sponsoring Agency Code
National Aeronautics and Space Administration Washington, D.C. 20546	

15. Supplementary Notes

Prepared for the 1985 Winter Annual Meeting of the American Society of Mechanical Engineers, Miami Beach, Florida, November 17-21, 1985.

16. Abstract

Analytical solutions for the three-dimensional inhomogeneous wave equation with flow in a hardwall rectangular wind tunnel and in the free field are presented for a stationary monopole noise source. Dipole noise sources are calculated by combining two monopoles 180° out of phase. Numerical calculations for the modal content, spectral response and directivity for both monopole and dipole sources are presented. In addition, the effect of tunnel alterations, such as the addition of a mounting plate, on the tunnels reverberant response are considered. In the frequency range of practical importance for the turboprop response, important features of the free field directivity can be approximated in a hardwall wind tunnel with flow if the major lobe of the noise source is not directed upstream. However, for an omnidirectional source, such as a monopole, the hardwall wind tunnel and free field response will not comparable.

17. Key Words (Suggested by Author(s))	18. Distribution Statement
Sound Propeller Monopole Flow	Unclassified - unlimited STAR Category 34

19. Security Classif. (of this report)	20. Security Classif. (of this page)	21. No. of pages	22. Price*
Unclassified	Unclassified		

*For sale by the National Technical Information Service, Springfield, Virginia 22161